Progress In Electromagnetics Research B, Vol. 59, 193–204, 2014

High-Frequency Method for Terahertz Radar Cross Section of Conductive Targets in Free Space

Houqiang Hua, Yuesong Jiang*, and Yuntao He

Abstract—The high-frequency method for the prediction of the terahertz (THz) radar cross section (RCS) of conductive targets with extremely electrically large size in free space was presented. In order to consider the scattering fields of the perfectly electric conducting (PEC) targets with extremely electrically large size in free space, the Green's function was introduced into the conventional physical optics (PO) method which was combined with the graphical electromagnetic computing (GRECO) method and improved using the partition display algorithm. The shadow regions were eliminated quickly by displaying lists of OpenGL to rebuild the targets, and the geometry information was attained by reading the color and depth of each pixel. The THz RCS of conductive targets can be exactly calculated in free space. The RCS comparison between the partition display GRECO prediction by the self-written Visual C++ 2010 program and the simulation of FEKO software with the large element PO method proves the validity and accuracy of the proposed method. The results provide an important basis and method for the potential applications of THz radar in many fields such as military, astronomy and remote sensing.

1. INTRODUCTION

The wavelength of terahertz (THz) wave is much shorter than that of microwave, so THz wave is suitable for the realization of great signal bandwidth and extremely narrow antenna beam, and conducive to the high-resolution imaging of targets. THz radar has important application prospects, especially in the bands of smaller atmospheric attenuation and space environment [1, 2]. Because the study on electromagnetic radiation and scattering properties of targets in THz band is an important basis for the future applications of THz radar, calculating the THz radar cross section (RCS) of targets with extremely electrically large size in free space has very important significance for national defense, aviation, aerospace, astronomy and remote sensing, etc., especially in missile system design and simulation, radar system design and identification. Whether in the developed argument of the new equipments or in the tactical use program formulation of the existing equipments, the analysis on RCSs and electromagnetic scattering properties of targets (such as aircrafts, ships, missiles, etc.) is necessary.

Various RCS prediction software packages based on high-frequency algorithms have been widely used for interactive modeling, computer-aided analysis and design optimization [3–5], such as the American Xpatch [6, 7], RadBase [8, 9], CADDSCAT [10], RECOTA [11], FISC [12, 13], British RESPECT [14], South African FEKO [15], Spanish graphical electromagnetic computing (GRECO) [16, 17] and RANURS [18]. In recent years, numerous scholars have adopted a variety of algorithms and softwares to compute the high-frequency RCSs of targets with electrically large size in free space and have obtained quite a lot good results. However, due to the constraints of the existing computer memory and computing time, the scattering problems of targets with extremely electrically large size are still unable to be better treated, and the targets' RCSs prediction calculations were limited

Received 27 January 2014, Accepted 4 April 2014, Scheduled 15 April 2014
* Corresponding author: Yuesong Jiang (yuesongjiang@buaa.edu.cn).
The authors are with the School of Electronic and Information Engineering, Beihang University, Beijing 100191, China.

to microwave or lower frequency bands in free space. So far, in the scope of the authors' knowledge, it has not been reported that the targets with extremely electrically large size in the THz band in free space were calculated by the high-frequency methods.

This paper focuses on the high-frequency method for RCS prediction of conductive targets with extremely electrically large size in the THz band in free space. Combining the physics optics (PO) analytical method in free space with the GRECO method and improved using the partition display algorithm, the THz RCSs of conductive targets with extremely electrically large size can be exactly calculated in free space. The RCS comparison between the partition display GRECO prediction by the self-written Visual C++ 2010 program and the simulation of FEKO software with the large element PO method shows that the proposed method is efficient and accurate. For illustration purposes, we limited our presentation to the monostatic case for perfectly electric conducting (PEC) targets in free space.

2. THEORETICAL METHOD

2.1. Target Far Field RCS Prediction Based on the PO and GRECO Methods

2.1.1. RCS of the Perfectly Conducting Surface Element

PO method is the name of a high-frequency approximation (short-wavelength approximation), which assigns a simple and clear value to the induced current on the scatterer's surface, replaces the scatterer itself with the surface current as the scattering source, and calculates the integral of the induced current on the surface to obtain the scattering field of the object. In the case of the perfect metal surface, we can derive the PO expression for the square root of the RCS according to the conventional PO method [19–21]:

$$\sqrt{\sigma} = -j\frac{k}{\sqrt{\pi}}\int_s \hat{n}\cdot\left(\hat{e}_r\times\hat{h}_i\right)\exp\left[jk\vec{r}\cdot\left(\hat{i}-\hat{s}\right)\right]ds \tag{1}$$

The integral can be evaluated exactly for only a handful of cases that include flat plates, cylinders, and spherical caps viewed at axial incidence. In the case of complex shape target, PO method is generally used to discretize complex surface into simple planes, such as rectangular or triangular flat plates, and then to predict the RCSs of the planes and to do the phase superposition in terms of the high-frequency characteristics of electromagnetic wave.

In GRECO method, the radar irradiation direction is perpendicular to the screen, i.e., it is the direction of $-\mathbf{z}$, and the radar scattering direction is the direction of $\mathbf{z}$. Thus, the scattering field can be changed to:

$$\sqrt{\sigma} = -\frac{jk}{\sqrt{\pi}}\int_s \cos\theta\cdot e^{2jkz}ds \tag{2}$$

where θ is the angle between the normal line and the incident ray of the conductor surface, z the distance between the surface element and the observation point. The integral field S is the illuminated region. The target figure processed in GRECO method is the projection of the target's three-dimensional surface on the computer screen. The integration element ds' on the computer screen can be expressed as $ds' = \cos\theta\cdot ds$. Therefore, the Formula (2) can be expressed as

$$\sigma = \frac{4\pi}{\lambda^2}\left|\int\cos\theta\cdot e^{2jkz}ds\right|^2 = \frac{4\pi}{\lambda^2}\left|\int\limits_{\text{screen}} e^{2jkz}ds'\right|^2 \tag{3}$$

In the calculation, Formula (3) can be discretized into:

$$\sigma = \frac{4\pi}{\lambda^2}\left|\sum_{\text{pixel}} e^{2jkz}\cdot\Delta s\right|^2 \tag{4}$$

where Δs is the area represented by each pixel on the screen and z the depth value extracted from the depth buffer. The surface element represented by each pixel is considered as a rectangular aperture plane

under uniform irradiation, and then the far-field effect can be approximated by the sinc function [22]. The discrete surface integral with PO method can be expressed as:

$$\sigma = \frac{4\pi}{\lambda^2}\left|\sum_{\text{pixel}} \text{sinc}\left(k\frac{l}{\cos\theta}\sin\theta\right)e^{2jkz}\cdot\Delta s\right|^2 \tag{5}$$

where l indicates the line length of a square pixel ds' on the screen and $l/\cos\theta$ the line length of the original target surface ds represented by the pixel.

According to the high frequency theories, the main contribution of curved surface's monostatic RCS lies in specular reflection point, whose normal vector is close to the incident direction. Because of the rapid changes in the phase, the physical optics surface integral calculated by numerical methods has some errors near the area at the junction of illuminated and shadowed area, and the effect can be multiplied by the gradually smaller function $\cos^n\theta$ because $\theta \to \pi/2$ at the shadow boundary. According to Formula (5), we can obtain:

$$\sigma = \frac{4\pi}{\lambda^2}\left|\sum_{\text{pixel}} \cos^n\theta\cdot\text{sinc}\left(k\frac{l}{\cos\theta}\sin\theta\right)e^{2jkz}\cdot\Delta s\right|^2 \tag{6}$$

where n is the parameter to control the effect of stationary phase approximation at the point. The surface integral of the object can be calculated strictly as discrete surfaces when $n = 0$, and the odd change effect can be eliminated when $n > 1$.

2.1.2. RCS of the Target Edge

The method of equivalent currents (MEC) can be used to solve edge scattering. We need to determine where the edges exist before calculating, firstly to judge whether there is a wedge between horizontally adjacent pixels on the same line in the screen, and then to judge whether there is a wedge between vertically adjacent pixels on the same column in the screen. The judgment process has two steps. The first is to determine whether the depth values of the two adjacent pixels are continuous, and the second is to determine whether the normal vectors of the pixels are different. When the depth values are continuous and the normal vectors are different, the junction of the surface elements represented by the two pixels is a edge.

According to the high frequency theories, the far scattered field of the edge can be regarded as the radiation of the equivalent line currents on it. The currents' magnitude is determined by the incident direction and the orientation of the observation point relative to the edge, and then the values along the edge are not constants. The equivalent currents are usually expressed as some functions of incremental length diffraction coefficients. Here the physical theory of diffraction (PTD) was used to calculate the edge diffraction coefficients, and then the MEC was used to calculate the backscattered field. The scattered field can be expressed as follows:

$$E^S_{\text{PTD}} = jk\frac{e^{jkr}}{4\pi R}\int\limits_L \left[\eta_0 I_e\hat{s}\times(\hat{s}\times\hat{t}) + I_m\hat{s}\times\hat{t}\right]\cdot e^{jkr\cdot s}dl \tag{7}$$

The above Equation (7) can be simplified and expressed as follows:

$$E_s = E_0\frac{e^{-jkr}}{2\pi r}\int\limits_l \left[-D_{||}\sin\gamma\hat{e}^i_{||} - D_x\cos\gamma\hat{e}^i_{||} - D_\perp\cos\hat{e}^i_\perp\right]\exp(2jkZ)dl' \tag{8}$$

where the line integral should be calculated along the edges illuminated by the incident wave. $\hat{e}^i_{||}$ and $\hat{e}^i_\perp$ are the unit vectors parallel and perpendicular to the incidence plane respectively which is determined by the directions of the incident ray and the edge. γ is the angle between the incident electric field and $\hat{e}^i_\perp$. $D_{||}$, $D_\perp$, D_x are the diffraction coefficients of monostatic incremental length.

In order to calculate the line integral of the equivalent line currents, the diffraction coefficients of incremental length must be calculated for each pixel in the edges, and the contributions of the pixels in

the edges should be added up. Because the coefficients are determined by α, β, φ, they can be solved by the following equations:

$$\alpha = \cos^{-1}(-n_1 \cdot n_2) \tag{9}$$

$$\sin\beta_r = \sqrt{t_x^2 + t_y^2} \tag{10}$$

$$\cos\varphi = \frac{n_{1x}t_y - n_{1y}t_x}{\sqrt{t_x^2 + t_y^2}} \tag{11}$$

$$\hat{t} = \frac{n_1 \times n_2}{|n_1 \times n_2|} \tag{12}$$

where $\hat{t}$ is a unit vector along the direction of the edge.

From the above formulas, we can deduce the monostatic edge scattering formulas in the GRECO method:

For horizontal polarization,

$$\sigma_{HH} = \frac{\Delta l^2}{\pi\lambda}\left|\sum_{\text{edge}}\left[-D_{||}\frac{t_x^2}{t_x^2+t_y^2} + D_x\frac{t_x t_y}{t_x^2+t_y^2} - D_{\perp}\frac{t_y^2}{t_x^2+t_y^2}\right]e^{2jkz}\right|^2 \tag{13}$$

For vertical polarization,

$$\sigma_{VV} = \frac{\Delta l^2}{\pi\lambda}\left|\sum_{\text{edge}}\left[-D_{||}\frac{t_y^2}{t_x^2+t_y^2} - D_x\frac{t_x t_y}{t_x^2+t_y^2} - D_{\perp}\frac{t_x^2}{t_x^2+t_y^2}\right]e^{2jkz}\right|^2 \tag{14}$$

2.1.3. RCS of the PEC Target

In high-frequency region, the scattering becomes a local effect, the interactions among the units of the scatterer significantly decrease. And every part of the object is essentially an independent scatterer, whose induced field depends only on the incident wave and is independent of the scattering energy of the other parts, so it is relatively simplified to calculate the induced field and the scattered field integral on the surface.

The total scattered field of a complex target can be composed of a superposition of the scattered fields of various independent scattering centers. The field of each scattering source is assumed to be the scattered field applied to the scattering combination, and the inter-shielding effect and multiple scattering among the scattering centers are ignored. So the RCS of the combination of N scattering centers can be given by the correlation superposition result from the sum of the relative phases:

$$\sigma = \left|\sum_{n=1}^{N}\sqrt{\sigma_n}\exp(j2kR_n)\right|^2 \tag{15}$$

where $2R_n$ is the two-way distance from the radar to the scattering center. The RCS of a complex target can be calculated by the relative phase superposition of the calculated RCS values of the components of the target.

2.2. Graphical Partition Display Algorithm

The GRECO method utilizes the computer's 3D graphics accelerator card to process the blanking of the target's invisible part, which can quickly obtain the pixels of the target's illuminated area, so can accelerate the RCS calculation to some extent. But the Z-Buffer blanking of the graphics accelerator card is performed in the image space, so the target's display precision must be subject to a limit of the image display resolution. When the incident direction is not perpendicular to the surface element, the display precision of the target affects both the amplitude and the phase of the scattered field calculation. The lower the display precision is, the greater the errors of the amplitude and phase of the scattered

field are, so the calculation accuracy of the RCS results is affected. For complex targets, when no larger surface elements of specular reflection exist, the pixel size must be smaller than $\lambda/20$ to get more accurate results of RCS calculation (λ is the wavelength) [22]. In this criterion, the target sizes accepted by the display resolution 1024×1280 are 64λ and 51λ in the x and y directions, respectively, i.e., 0.192 m and 0.153 m when the frequency of the incident wave is 100 GHz, which are much smaller than the actual sizes of the general complex targets. So the realistic resolution of the graphics accelerator card itself does not meet the needs of the real complex targets' RCS accurate calculation in the high-frequency region.

In the graphical partition display algorithm, the target's projection is divided into a plurality of areas, and only one of these areas is displayed each time, which is equivalent to that the image is amplified to achieve the desired display accuracy requirement of RCS calculation. Therefore, the graphical partition display algorithm is an effective method to solve the problem of the display resolution limitation in GRECO method.

The hardware limitation of monitor resolution can be broken by OpenGL projection functions. The projections of OpenGL are perspective projection and orthogonal projection, and only the orthogonal projection can be used in the GRECO method because the perspective projection will cause the target model's deformation. A perpendicular parallelepiped is defined by the orthogonal projection function, and all parts of the model outside the hexahedron will be clipped and not displayed. Therefore, the target can be displayed on the screen with many screens by setting the parameters of the orthogonal projection function. Only part of the target will be displayed, and the other parts clipped out will not be calculated each time. Finally, the RCS of the target can be obtained by the superposition of the results of the calculation each time. As shown in Figure 1, the sphere target was displayed with two screens by setting the parameters of the orthogonal projection function.

The graphical partition display algorithm increases the resolution used in the GRECO method to make the target displayed more accurately, so that the accuracy of RCS prediction of the target was improved. The subdivision situation of the target model has changed after the resolution was increased. Figure 2 shows the screenshots of the calculation of the sphere target in four screens. As shown in Figure 2, the target unit which originally occupied 2×2 pixels on the monitor now occupies 4×4 pixels.

The first thing we need to do is to determine the target's projection sizes (i.e., the sizes in the x, y-axis directions) at the current posture in the graphical partition display algorithm. Second, according to the size of a given pixel resolution, the projection rectangle is divided along the x, y-axis directions to obtain multiple partitions, and then a separate projection display is made for each partition. So the total field can be obtained by the superposition of the scattered fields of each partition, and then the RCS of the complex target can be predicted.

It should be noted that although the partition display and more detailed subdivision of the target model can improve the prediction accuracy, the run time of the program and the required memory size for the calculation are proportional to the detail level of the target's mesh file in the process of

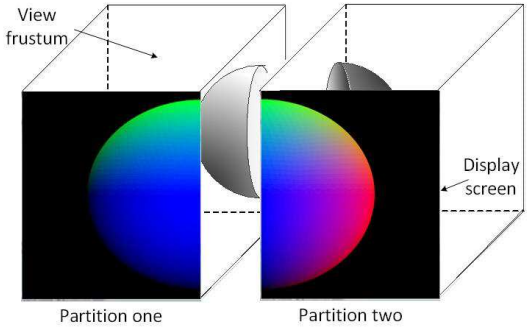

Figure 1. Sphere target displayed with two screens by setting the parameters of the orthogonal projection function.

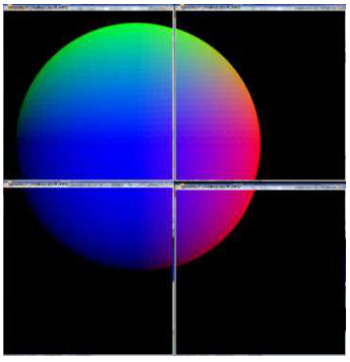

Figure 2. Screenshots of sphere target computed in four screens.

rasterization and proportional to the number of pixels occupied by the target when calculating RCS with the PO and GRECO methods.

3. NUMERICAL RESULTS AND DISCUSSION

When the objects are calculated with the PO and GRECO methods from the simple targets to the complex ones with extremely electrically large size in free space, CPU time for RCS prediction is spent only on the electromagnetic computation, whereas the more time-consuming geometric model manipulations are left to the graphics hardware. Whether the targets are simple or complex, the scattered field of each illuminated pixel is calculated in the same way. That the objects calculated are generalized from the simple targets to the complex ones will only increase the computational workload of the OpenGL's shadowing judgment on the targets. Combined with the free-space Green's function, the high-frequency approximation to RCS prediction is easily computed from the knowledge of the unit normals at the illuminated surfaces of the targets in free space.

FEKO software is a simulation tool for electromagnetic field analysis of 3D structure. For the targets with extremely electrically large size, accurate analysis methods often require a lot of memory resources. FEKO offers a variety of hybrid high-frequency algorithms that can be used to analyze the RCSs of the targets with extremely electrically large size easily, quickly and accurately. And FEKO has introduced the solution technique of large element PO since version 6.0 [15], which can be combined with the small surface element PO method and the method of moments (MOM), enhances the scattering computation ability of handling metal, dielectric and metal/dielectric mixed targets with extremely electrically large size, and reduces the computing resource requirements by the large grid subdivision of the targets' models. In the THz band, the targets such as aircrafts, missiles and ships belong to the targets with extremely electrically large size. Thus, FEKO is more suitable for this research among a variety of commercial electromagnetic analysis softwares. In order to test the correctness of the far-field RCS calculation algorithm for typical standard body objects or complex military targets at the frequency greater than or equal to 0.3 THz and the program written by the Visual C++ 2010 software, the results calculated by the Visual C++ program can be compared with the FEKO software simulation results with the large element PO method. The following examples were all calculated by the DELL Precision T7600 graphics workstation, which was specifically configured to: the CPU is 2× Intel Xeon E5-2680 0@2.70 GHz; the memory is 128 GB; the graphics card is Nvidia Quadro 5000; the monitor resolution is 1920×1200.

The coordinate system of the scattered field was defined firstly to facilitate the subsequent calculations. As shown in Figure 3, in the Cartesian coordinate system O-xyz, the angle formed by the radar's line of sight (LOS) (i.e., the incident direction from the radar to the target or the scattering direction from the target to the receiving radar) and the z-axis is the radar scan angle (i.e., aspect angle) θ, and the angle formed by the projection of the radar's LOS on the x-y plane and the x-axis is the azimuth angle φ.

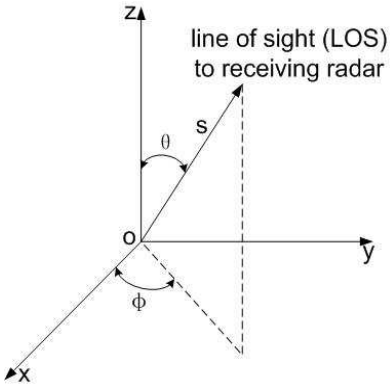

Figure 3. Schematic diagram of the coordinate system of the scattered field.

3.1. RCS of the Canonical Geometry Target

First, the THz RCSs of the conductive simplified canonical geometry targets with extremely electrically large size — ball and flat plate in free space were calculated with the partition display GRECO method below. And the results calculated by the self-written Visual C++ 2010 program can be compared with the simulation results of FEKO software with the large element PO method to test the correctness of the algorithm and the program. Then the calculated target was generalized to the typical complex military target with extremely electrically large size — the mother warhead of the Minuteman III intercontinental ballistic missile.

Figure 4 shows the geometry of a perfectly conducting sphere in free space whose diameter is 1 m and the incident waves added to the sphere. As shown in Figure 4, the center of the sphere lies at the origin of the coordinate system. The sphere's RCS characteristics do not change with the changes in azimuth angle φ because of the symmetry of the sphere, so we may assume $\varphi = 0°$. Let the aspect angle θ be varied from 0° to 180° and the calculated interval be 2°. The calculated frequency was 400 GHz; the electrical length was diameter 1333λ; the pixel subdivision accuracy was 0.3λ. The results of the sphere's RCS calculation are shown in Figure 5. In Figure 5, the (black) solid line with asterisks, the (red) dash line plus crosses and the (blue) dash-dot line denote the change graphs of the sphere's RCS with the aspect angle θ obtained using the Visual C++ program with the partition display GRECO method, the FEKO software with the large element PO method and by Mie scattering theory, respectively.

Figure 5 shows the perfectly conducting sphere's RCS comparison of the partition display GRECO prediction, the simulation of FEKO software with the large element PO method and the calculated values by Mie scattering theory at a fixed frequency 400 GHz. There is good fit between the prediction of the derivated partition display GRECO method and the simulation of FEKO software for vertical polarization, and there are noticeable differences within 1 dBsm. In Figure 5, we can also see that the agreement between the partition display GRECO prediction and the calculated values by Mie theory is almost perfect with noticeable differences within 0.2 dBsm, and the result of the partition display GRECO prediction is better than the simulation of FEKO software with respect to the calculated values by Mie theory.

Figure 6 shows the geometry of a perfectly conducting flat plate in free space whose size is 1 m × 1 m and the incident waves added to the flat plate. As shown in Figure 6, the center of the flat plate lies at the origin of the coordinate system. Assume the azimuth angle $\varphi = 0°$. Let the aspect angle θ be varied from 0° to 180° and the calculated interval be 2°. The calculated frequency was 400 GHz; the electrical length was $1333\lambda \times 1333\lambda$; the pixel subdivision accuracy was 0.3λ. The results of the flat

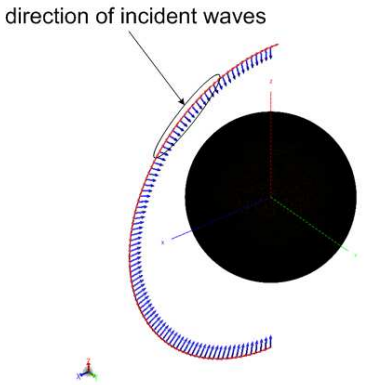

Figure 4. Schematic diagram of the incident waves to a conducting sphere with a 1 m diameter.

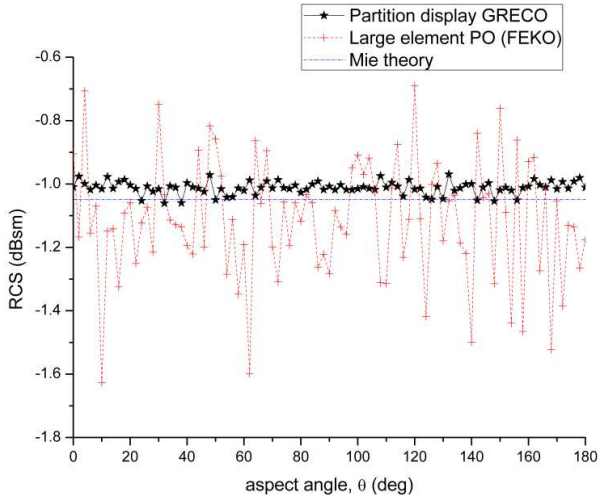

Figure 5. Sphere RCS comparison of the partition display GRECO prediction, the simulation of FEKO software and the calculated values by Mie theory (vertical polarization).

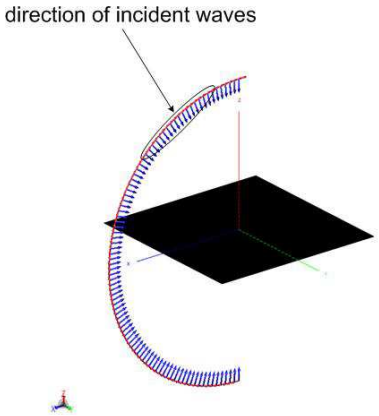

Figure 6. Schematic diagram of the incident waves to the 1 m × 1 m flat plate.

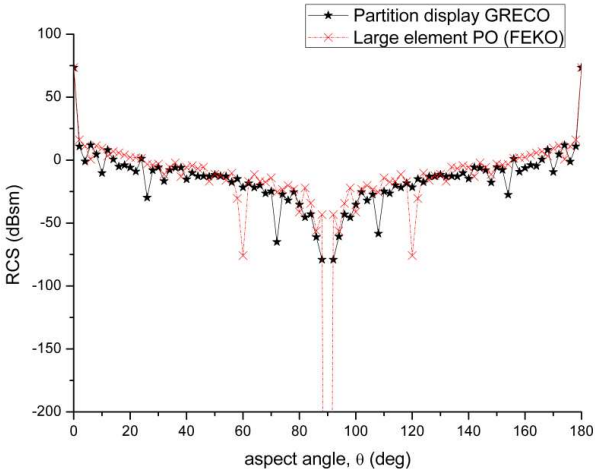

Figure 7. Flat plate RCS comparison of the partition display GRECO prediction and the simulation of FEKO software (vertical polarization).

plate's RCS calculation were shown in Figure 7. In Figure 7, the (black) solid line with asterisks and the (red) dash-dot line plus crosses denote the change graphs of the flat plate's RCS with the aspect angle θ obtained using the Visual C++ program with the partition display GRECO method and the FEKO software with the large element PO method respectively.

Figure 7 shows the perfectly conducting flat plate's RCS comparison of the partition display GRECO prediction and the simulation of FEKO software with the large element PO method at a fixed frequency 400 GHz. There is good fit between the prediction of the derivated partition display GRECO method and the simulation of FEKO software for vertical polarization, except for the flash produced by the leading edge of the flat plate in total prediction. The discrepancy is caused by the currents induced on the facet's free edges.

3.2. RCS of the Mother Warhead of the Minuteman III Intercontinental Ballistic Missile

The calculated target was generalized to the typical complex military target with extremely electrically large size — the mother warhead of the Minuteman III intercontinental ballistic missile below. The following is to calculate the THz RCS of the mother warhead of the Minuteman III intercontinental ballistic missile in free space.

The strategic or tactical ballistic missile generally consists of two major components which are warhead (i.e., nosecone) and missile body (i.e., other parts of the missile). Among them, the warhead and missile body of the medium-range and short-range ballistic missile are not separated during flighting, and the warhead and missile body of the remote or strategic ballistic missile are separated after the completion of the boost phase to reduce the RCS when re-entering the atmosphere, and the missile body is detonated to form false targets of the missile body's fragments. Therefore, different simulation strategies should be considered for different ballistic missiles, e.g., for the remote or strategic ballistic missile, only the warhead's RCS characteristics of the target should be considered after the midcourse, and for the medium-range and short-range ballistic missile, the whole missile body's RCS characteristics of the target should be considered. Thus, for the Minuteman III intercontinental ballistic missile, only the warhead's RCS characteristics should be considered after the midcourse, and it is unnecessary to consider the whole missile body's RCS characteristics, which has the practical significance. Minuteman III intercontinental ballistic missile is shown in Figure 8.

The MK-12 mother warhead of the Minuteman III intercontinental ballistic missile is ogival, whose length is 3.66 m and bottom diameter 1.32 m [23], and it can be simplified as the composition of an elongated truncated cone at the bottom and a spheroid at the top. Figure 9 shows the geometry of the mother warhead of the Minuteman III intercontinental ballistic missile in free space and the incident

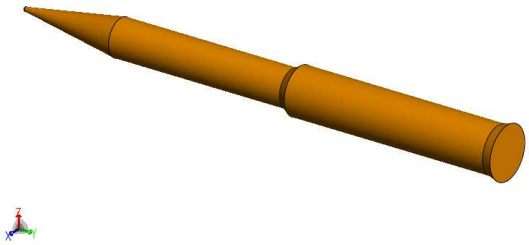

Figure 8. Geometry of Minuteman III intercontinental ballistic missile.

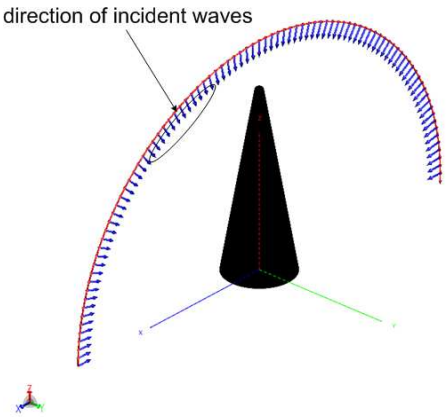

Figure 9. Schematic diagram of the incident waves to the Minuteman III intercontinental ballistic missile warhead.

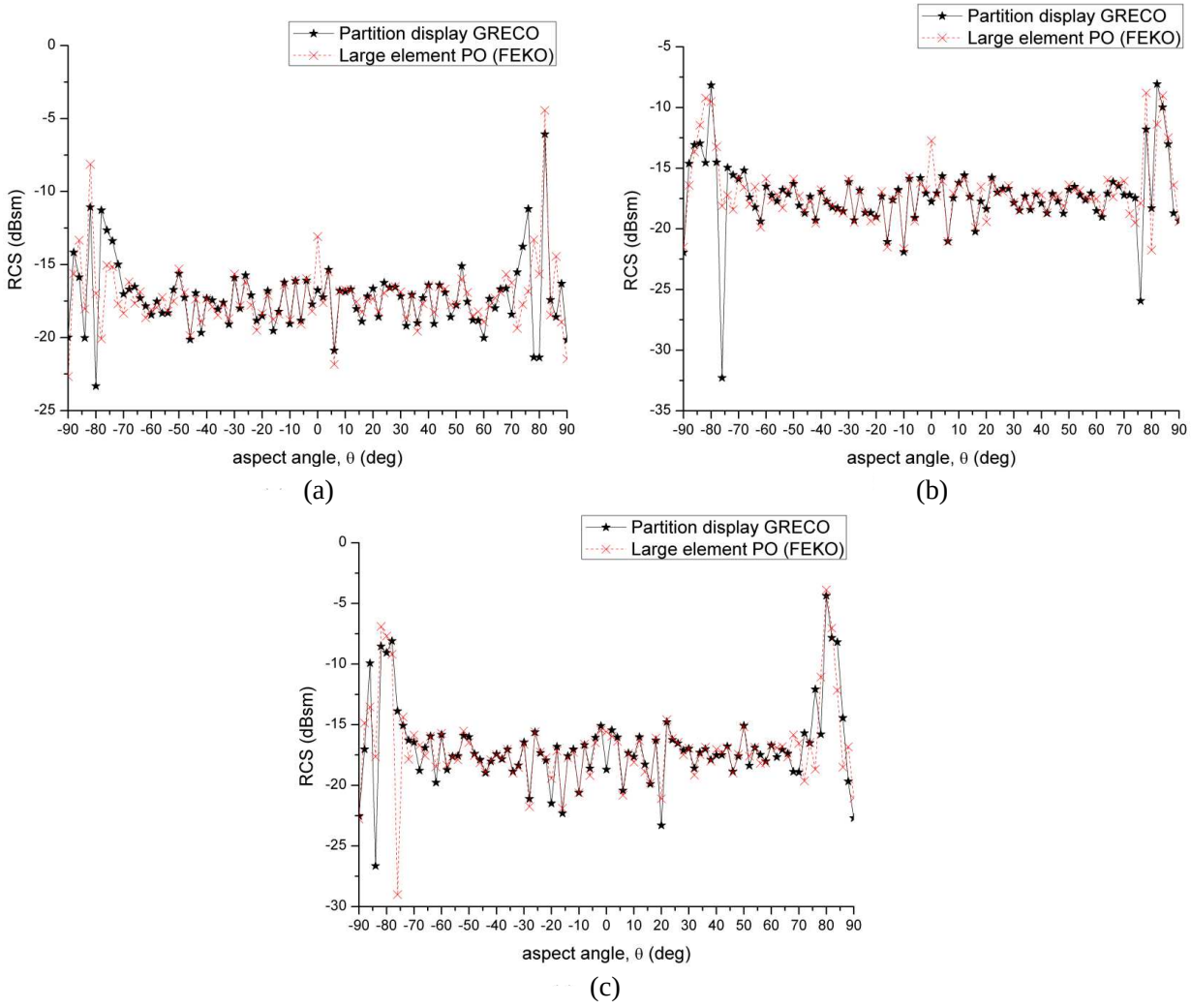

Figure 10. Change graphs of the warhead RCS of Minuteman III intercontinental ballistic missile with aspect angle. (a) $f = 350\,\text{GHz}$. (b) $f = 400\,\text{GHz}$. (c) $f = 450\,\text{GHz}$.

waves added to the mother warhead of the Minuteman III intercontinental ballistic missile. As shown in Figure 9, the center of the circular flat end of the warhead lies at the origin of the coordinate system. The warhead's RCS characteristics do not change with the changes in azimuth angle φ because of the symmetry of the warhead, so we may assume $\varphi = 0°$. Let the the aspect angle θ be varied from $-90°$ to $90°$ and the calculated interval be $2°$. When the calculated frequencies were 350 GHz, 400 GHz and 450 GHz, the electrical sizes were length 4270λ and bottom diameter 1540λ, length 4880λ and bottom diameter 1760λ, length 5490λ and bottom diameter 1980λ, respectively. The pixel subdivision accuracy was 0.3λ. The results of the warhead's RCS calculation were shown in Figure 10. In Figure 10, the (black) solid line with asterisks and the (red) dash line plus crosses denote the change graphs of the Minuteman III intercontinental ballistic missile warhead's RCS with the aspect angle θ obtained using the Visual C++ program with the partition display GRECO method and the FEKO software with the large element PO method respectively.

As can be seen from Figure 10, there is good fit between the prediction of the partition display GRECO method and the simulation of FEKO software with the large element PO method for vertical polarization at the fixed frequencies of 350 GHz, 400 GHz and 450 GHz. The trend of the curves has good consistency, and the accuracy can ensure the requirements of the RCS calculations. This proves that the prediction of the THz RCS of the typical complex military target with extremely electrically large size — the mother warhead of the Minuteman III intercontinental ballistic missile is efficient and accurate, which was based on the PO and GRECO methods and improved using the partition display algorithm.

When the direction of the incident wave of the radar is facing the top of the mother warhead of the Minuteman III intercontinental ballistic missile, the aspect angle θ is $0°$. For this special case, the RCS of the spherical-top cone has a credible theoretical analytic formula $\sigma = \pi r^2 + \lambda^2(\tan\alpha)^4/16\pi$, where r is the radius of the top sphere and α the half-angle of the bottom cone [24, 25]. Assume the azimuth angle $\varphi = 0°$, let the calculated frequency be varied from 350 GHz to 450 GHz and the calculated interval be 5 GHz. The pixel subdivision accuracy was 0.3λ. The RCS results of the warhead when illuminated facing the top were shown in Figure 11. In Figure 11, the (black) solid line with asterisks, the (blue) dash line plus triangles and the (red) dotted line plus diamonds denote the change graphs of the Minuteman III intercontinental ballistic missile warhead's RCS with the frequency for normal incidence obtained using the Visual C++ program with the partition display GRECO method, the theoretical analytical formula and the FEKO software with the large element PO method respectively.

As can be seen from Figure 11, there is good fit between the prediction of the partition display GRECO method and the numerical results calculated with the theoretical analytic formula with the frequency varied from 350 GHz to 450 GHz for normal incidence and the maximum error less than

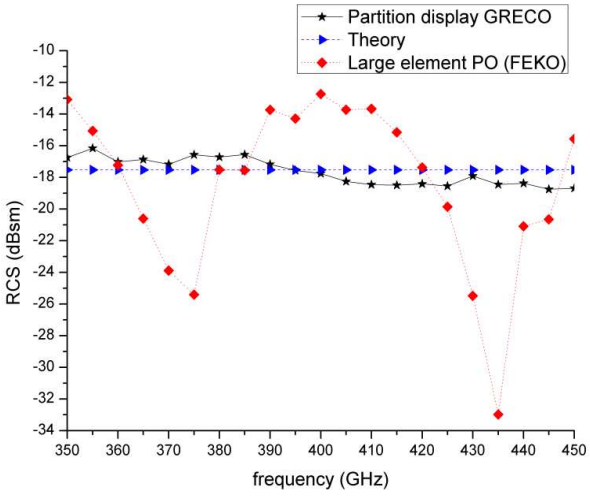

Figure 11. Change graphs of the warhead RCS of Minuteman III intercontinental ballistic missile with frequency for normal incidence.

1.5 dBsm, which can ensure the accuracy of the RCS computing requirements. The simulation results of FEKO software with the large element PO method match well with the numerical results calculated with the theoretical analytic formula only at the small part of frequency points, and have a greater difference relative to the prediction of the partition display GRECO method at most of the frequency points, so the simulation results of FEKO software are relatively inaccurate here. This proves that the partition display GRECO method can work better for the prediction of the THz RCS of the above typical complex military target with extremely electrically large size — the mother warhead of the Minuteman III intercontinental ballistic missile than the FEKO software with the large element PO method. The research results can provide a useful reference and technical support for the active spaceborne sensors to detect mid-flight ballistic missiles.

4. CONCLUSION

Combined the PO method in free space with the GRECO method and improved using the partition display algorithm, the shadow regions were eliminated by displaying lists technology of OpenGL to rebuild the target, and the geometric information was obtained by reading the color and depth of each pixel. The THz RCSs of the conductive typical simple and complex targets with extremely electrically large size can be exactly calculated in free space. The numerical results show that the prediction of the partition display GRECO method is efficient and accurate. The research results can provide an important basis and method for the future applications of THz radar in the fields of military, astronomy and remote sensing.

ACKNOWLEDGMENT

This work was supported by the National Natural Science Foundation of China (NSFC) under Grant No. 61101154.

REFERENCES

1. Li, H. Y., Q. Li, K. Xue, et al., "Research into influence of Gaussian beam on terahertz radar cross section of a conducting cylinder," *Journal of Infrared, Millimeter, and Terahertz Waves*, Vol. 34, Nos. 3–4, 289–298, 2013.
2. Li, H. Y., Q. Li, Z. W. Xia, et al., "Influence of Gaussian beam on terahertz radar cross section of a conducting sphere," *Journal of Infrared, Millimeter, and Terahertz Waves*, Vol. 34, No. 1, 88–96, 2013.
3. Li, X. F., Y. J. Xie, and R. Yang, "High-frequency method for scattering from coated targets with electrically large size in half space," *IET Microw. Antennas Propag.*, Vol. 3, No. 2, 181–186, 2009.
4. Li, X. F., Y. J. Xie, and R. Yang, "High-frequency method analysis on scattering from homogenous dielectric objects with electrically large size in half space," *Progress In Electromagnetics Research B*, Vol. 1, 177–188, 2008.
5. Li, X. F., Y. J. Xie, P. Wang, et al., "High-frequency method for scattering from electrically large conductive targets in half-space," *IEEE Antennas and Wireless Propagation Letters*, Vol. 6, 259–262, 2007.
6. Hazlett, M. A., D. J. Andersh, S. W. Lee, et al., "XPATCH: A high frequency electromagnetic scattering prediction code using shooting and bouncing rays," *Proc. SPIE, Targets and Backgrounds: Characterization and Representation*, Vol. 2469, 266–275, 1995.
7. Andersh, D. J., J. Moore, S. Kosanovich, et al., "Xpatch 4: The next generation in high frequency electromagnetic modeling and simulation software," *Proc. of the IEEE International Radar Conference*, 844–849, 2000.
8. Zhou, M. J., J. Lu, Q. Chang, et al., "SAR image simulation systems based on RadBase and Vega," *Modern Radar*, Vol. 31, No. 3, 27–30, 2009.

9. Yuan, X., T. Tang, Y. Li, et al., "SAR image classification by image intensity similarity and kernel method," *Proc. of the 5th IEEE International Congress on Image and Signal Processing (CISP)*, 1386–1389, 2012.
10. Roedder, J. M., "CADDSCAT Version 2.3: A high-frequency physical optics code modified for trimmed IGES B-spline surfaces," *IEEE Antennas and Propagation Magazine*, Vol. 41, No. 3, 69–80, 1999.
11. Youssef, N. N., "Radar cross section of complex targets," *Proc. of the IEEE*, Vol. 77, No. 5, 722–734, 1989.
12. Song, J. M., C. C. Lu, W. C. Chew, et al., "Fast Illinois solver code (FISC)," *IEEE Antennas and Propagation Magazine*, Vol. 40, No. 3, 27–34, 1998.
13. Song, J. M. and W. C. Chew, "Large scale computations using FISC," *Proc. of the IEEE Antennas and Propagation Society International Symposium*, Vol. 4, 1856–1859, 2000.
14. Turner, S. D., "RESPECT: Rapid electromagnetic scattering predictor for extremely complex targets," *IEE Proceedings F (Radar and Signal Processing)*, Vol. 137, No. 4, 214–220, 1990.
15. FEKO, "Comprehensive electromagnetic solutions," Accessed Dec. 16, 2013, Available: http://www.feko.info.
16. Rius, J. M., M. Ferrando, and L. Jofre, "High-frequency RCS of complex radar targets in real-time," *IEEE Trans. Antenn. Propag.*, Vol. 41, No. 9, 1308–1319, 1993.
17. Rius, J. M., M. Ferrando, and L. Jofre, "GRECO: Graphical electromagnetic computing for RCS prediction in real time," *IEEE Antennas and Propagation Magazine*, Vol. 35, No. 2, 7–17, 1993.
18. Domingo, M., F. Rivas, J. Perez, et al., "Computation of the RCS of complex bodies modeled using NURBS surfaces," *IEEE Antennas and Propagation Magazine*, Vol. 37, No. 6, 36–47, 1995.
19. Knott, E. F., "A progression of high-frequency RCS prediction techniques," *Proc. of the IEEE*, Vol. 73, No. 2, 252–264, 1985.
20. Knott, E. F., *Radar Cross Section,* 183–224, SciTech Publishing, North Carolina, 2004.
21. Ruan,Y. Z., *Radar Cross Section and Stealth Technology,* National Defense Industry Press, Beijing, 1998.
22. Nie, Z. P. and D. G. Fang, *Target and Environment Electromagnetic Scattering Modeling: Theory, Methodology and Implementation,* Applications Chapter, 202–228, National Defense Industry Press, Beijing, 2009.
23. Zhu, K. L. and W. X. Wang, *Missile Encyclopedic Dictionary,* 34–38, China Astronautic Publishing House, Beijing, 2001.
24. Crispin, J. W. and A. L. Maffett, "Radar cross-section estimation for simple shapes," *Proc. of the IEEE*, Vol. 53, No. 8, 833–848, 1965.
25. Crispin, J. W. and A. L. Maffett, "Radar cross-section estimation for complex shapes," *Proc. of the IEEE*, Vol. 53, No. 8, 972–982, 1965.